

# Density-Matrix Theory of Quantum Dynamics under a Strong External Field Switched on Nonadiabatically

Hikaru Kitamura<sup>1</sup>

<sup>1</sup> Hikaru Kitamura

Department of Physics, Kyoto University, Sakyo-ku, Kyoto 606-8502, Japan

E-mail: kitamura@scphys.kyoto-u.ac.jp

## ABSTRACT

Quantum time-evolution equations for the density matrix are formulated in the unrestricted Hartree-Fock approximation, with an emphasis on the nonperturbative effect due to a sudden or gradual onset of a strong external field. Numerical simulations are performed for ideal Fermi gas around a square-well potential which is switched on dynamically. When the switching is fast enough, an oscillatory motion of the particle is induced by a nonadiabatic transition at the Landau-Zener crossing point, which is most clearly seen in a small-size system. When the switching is sufficiently slow, the simulation corroborates the adiabatic theorem. It is shown that the Anderson's infrared catastrophe in a metal is strongly enhanced by the nonperturbative effect. The Keldysh formula of atomic multiphoton ionization can also be derived from the nonperturbative term in the density-matrix equation, indicating a wide applicability of the present theory.

## Introduction

The dynamics of quantum particles in a suddenly applied external field has been an important subject in atomic, molecular, and condensed-matter science. The state-of-the-art vacuum ultraviolet or x-ray free electron lasers<sup>[1]</sup> can excite deep core electrons in a material within a femtosecond time scale; dynamic response of surrounding electrons to rapidly evolving core-hole potentials is a key issue in the analysis of the experimental data.<sup>[2]</sup> When a certain Bardeen-Cooper-Schrieffer (BCS)-type superconductor is excited suddenly by an intense terahertz laser pulse, a transient oscillation of the order parameter is observed, whose frequency coincides with the asymptotic BCS gap energy.<sup>[3,4]</sup> Multiphoton or tunneling ionization of an atom or molecule is another notable nonlinear phenomenon induced by a strong laser field.<sup>[5,6]</sup>

Generally, the transitions between quantum states triggered by a sudden change in the external potential are called *nonadiabatic transitions*.<sup>[7]</sup> Oppositely, when an external

potential is turned on sufficiently slowly, each eigenstate of the initial Hamiltonian joins continuously into the corresponding eigenstate of the new Hamiltonian, known as the *adiabatic theorem*.<sup>[8]</sup> Comprehensive elucidation of quantum dynamics over a wide range of adiabaticity is a fundamental issue of significance.

In this article, we develop a density matrix theory of quantum dynamics in the time-dependent unrestricted Hartree-Fock (TDUHF) approximation,<sup>[9-11]</sup> where a special attention is paid to the nonperturbative effects due to a suddenly or gradually applied external field. As an illustrative example, numerical simulations are performed for an ideal Fermi gas when a square-well potential is switched on with an arbitrary time constant  $\tau$ . We thus show that the nonperturbative effect gives rise to rich phenomena such as an oscillatory motion in the nonadiabatic (small- $\tau$ ) regime as well as the enhancement of Anderson's infrared catastrophe<sup>[12-14]</sup> in the adiabatic (large- $\tau$ ) regime. Finally, we show that the Keldysh formula for atomic multiphoton ionization<sup>[5]</sup> can

be derived from the nonperturbative term in the density-matrix equation.

## Density-Matrix Formalism

We consider a general many-electron (or many-Fermion) system. In the initial state ( $t = 0$ ), where the external field is absent, we suppose that the wave functions  $\psi_{k\sigma}^{(0)}(\mathbf{r})$  and energy levels  $\varepsilon_{k\sigma}^{(0)}$  for one-electron state  $k$  and spin  $\sigma$  are already known through the static unrestricted Hartree-Fock (UHF) calculation.

The external field  $v_{\text{ext}}(\mathbf{r}, t)$  is switched on at  $t=0$ . The subsequent dynamics of the system can be computed with the TDUHF equation for the one-particle wave function  $\psi_{m\sigma}(\mathbf{r}, t)$ ; [9,11] equivalently, we can simulate the one-particle density matrix,

$$\langle \rho_{kk'\sigma}(t) \rangle \equiv \sum_{m=1}^{\text{occ}} \langle \psi_{k'\sigma}^{(0)} | \psi_{m\sigma}(t) \rangle \langle \psi_{m\sigma}(t) | \psi_{k\sigma}^{(0)} \rangle, \quad (1)$$

where the summation is taken over all occupied states. [9]

The diagonal component  $f_{k\sigma}(t) \equiv \langle \rho_{kk\sigma}(t) \rangle$  represents the average occupation number of state  $\{k, \sigma\}$ ; it obeys the Heisenberg equation of motion [10]

$$\frac{\partial f_{k\sigma}(t)}{\partial t} = \frac{2}{\hbar} \text{Im} \sum_{k'(\neq k)} \left[ \tilde{\varepsilon}_{kk'\sigma}(t) + (v_{\text{ext}}(t))_{kk'\sigma} \right] \langle \rho_{kk'\sigma}(t) \rangle. \quad (2a)$$

The corresponding equation for the off-diagonal component ( $k \neq k'$ ) reads

$$\begin{aligned} i\hbar \frac{\partial \langle \rho_{kk'\sigma}(t) \rangle}{\partial t} &= (\varepsilon_{k'\sigma}^{(0)} - \varepsilon_{k\sigma}^{(0)}) \langle \rho_{kk'\sigma}(t) \rangle \\ &+ \left[ \tilde{\varepsilon}_{k'k'\sigma}(t) - \tilde{\varepsilon}_{kk\sigma}(t) + (v_{\text{ext}}(t))_{k'k'\sigma} - (v_{\text{ext}}(t))_{kk\sigma} \right] \\ &\quad \times \langle \rho_{kk'\sigma}(t) \rangle \\ &+ \left[ \tilde{\varepsilon}_{k'k\sigma}(t) + (v_{\text{ext}}(t))_{k'k\sigma} \right] [f_{k\sigma}(t) - f_{k'\sigma}(t)] \\ &+ \sum_{q(\neq k, k')} \left[ \left( \tilde{\varepsilon}_{k'q\sigma}(t) + (v_{\text{ext}}(t))_{k'q\sigma} \right) \langle \rho_{kq\sigma}(t) \rangle \right. \\ &\quad \left. - \left( \tilde{\varepsilon}_{qk\sigma}(t) + (v_{\text{ext}}(t))_{qk\sigma} \right) \langle \rho_{qk'\sigma}(t) \rangle \right]. \quad (2b) \end{aligned}$$

Note that Eq. (2a) duly satisfies the particle-number conservation,  $\sum_{k\sigma} (\partial f_{k\sigma} / \partial t) = 0$ . We also remark that  $\langle \rho_{kk'\sigma}(0) \rangle = 0$  for  $k \neq k'$ , since both  $k$  and  $k'$  are eigenstates of the initial (unperturbed) Hamiltonian.

In Eqs. (2a) and (2b), we have introduced a matrix element of the external potential,

$$(v_{\text{ext}}(t))_{kk'\sigma} \equiv \int d\mathbf{r} \psi_{k\sigma}^{(0)*}(\mathbf{r}) v_{\text{ext}}(\mathbf{r}, t) \psi_{k'\sigma}^{(0)}(\mathbf{r}). \quad (3)$$

It induces a transition between different  $k$ -states, which in turn modifies the Hartree and exchange interactions among electrons. Such a change is described by the self-energy matrix, [10]

$$\begin{aligned} \tilde{\varepsilon}_{kk'\sigma}(t) &\equiv \sum_{k_1 k_2 \sigma_1} \left( V_{kk'k_1 k_2}^{\sigma\sigma_1} - \delta_{\sigma\sigma_1} V_{kk_2 k_1 k'}^{\sigma\sigma} \right) \\ &\quad \times \left[ \langle \rho_{k_1 k_2 \sigma_1}(t) \rangle - \delta_{k_1 k_2} f_{k_1 \sigma_1}(0) \right], \quad (4) \end{aligned}$$

with the Coulomb repulsion integral,

$$\begin{aligned} V_{k_1 k_2 k_3 k_4}^{\sigma\sigma'} &\equiv \int d\mathbf{r}_1 \int d\mathbf{r}_2 \psi_{k_1 \sigma}^{(0)*}(\mathbf{r}_1) \psi_{k_2 \sigma}^{(0)}(\mathbf{r}_1) \\ &\quad \times \frac{e^2}{|\mathbf{r}_1 - \mathbf{r}_2|} \psi_{k_3 \sigma'}^{(0)*}(\mathbf{r}_2) \psi_{k_4 \sigma'}^{(0)}(\mathbf{r}_2). \quad (5) \end{aligned}$$

Note that  $\tilde{\varepsilon}_{kk'\sigma}(0) = 0$  by definition.

Density-matrix formulations of TDUHF equations have been known for many years, [9,11] but Eqs. (2a) and (2b) differ from the previous expressions in a sense that the matrix elements are evaluated with the unperturbed UHF wave functions in the initial state. The present formalism would therefore be suitable for solving an initial-value problem after the external field is switched on.

The nonlinear term ( $q \neq k, k'$ ), that is, the last term on the right-hand side of Eq. (2b), accounts for a nonperturbative effect, which is our primary concern. This term was ignored in our previous work, [10] where the density matrix equations were converted into the rate equations within the Markov approximation.

The total energy at time  $t$  can be evaluated as

$$E_{\text{tot}}(t) = \sum_{k\sigma} \varepsilon_{k\sigma}^{(0)} f_{k\sigma}(t) + \sum_{kk'\sigma} \left[ (v_{\text{ext}}(t))_{kk'\sigma} - \frac{1}{2} W_{kk'\sigma} + \frac{1}{2} \tilde{\varepsilon}_{kk'\sigma}(t) \right] \langle \rho_{kk'\sigma}(t) \rangle, \quad (6)$$

where

$$W_{kk'\sigma} \equiv \sum_{k_1\sigma_1} \left( V_{kk'_1k_1}^{\sigma\sigma_1} - \delta_{\sigma\sigma_1} V_{kk_1k_1}^{\sigma\sigma} \right) f_{k_1\sigma_1}(0). \quad (7)$$

At  $t=0$ , Eq. (6) appropriately reproduces the static UHF total energy in the unperturbed state.

When the present method is applied to a realistic molecule, the initial molecular orbitals  $\psi_{k\sigma}^{(0)}(\mathbf{r})$  can be expressed in the form of a linear combination of atomic orbitals as usual, but they should be computed up to sufficiently high-lying excited states in order for an accurate simulation of the subsequent electron dynamics. The number of two-electron integrals (5) may become fairly large, but they are independent of time and hence computed only once.

While the time-dependent density-functional theory (TDDFT) may be computationally more efficient,<sup>[15]</sup> an advantage of the TDUHF theory is an absence of self-interaction errors, owing to the rigorous treatment of the nonlocal exchange potential in the latter. The density-matrix equation can be derived exactly from the first-principles Hamiltonian and hence the formulation is straightforward in the Hamiltonian-based TDUHF theory, in contrast to the TDDFT which is based on the free-energy functional. In principle, the electron correlation effects beyond UHF can be incorporated into Eqs. (2a) and (2b) through collision integrals.<sup>[10]</sup>

## Nonadiabatic Switching of a Square-Well Potential

As an illustrative application of the density-matrix equations, we consider  $N$  free Fermions

of mass  $m$  confined in a spherical box of radius  $R$ , for which the Coulomb repulsion integrals (5) are neglected. The unperturbed energy eigenvalues and wave functions are written as<sup>[12]</sup>

$$\varepsilon_{k\sigma}^{(0)} = \frac{\hbar^2 k^2}{2m}, \quad \psi_{k\sigma}^{(0)}(\mathbf{r}) = \frac{1}{\sqrt{2\pi R}} \frac{\sin(kr)}{r},$$

$$k = \frac{n\pi}{R} \quad (n=1, 2, 3, \dots), \quad (8)$$

where we consider only s-waves because of the symmetry. A spherically symmetric square-well potential of radius  $a_0$  is switched on at time  $t = 0$  and its depth grows toward a constant value  $V_0$  for  $t \rightarrow \infty$ . In terms of the distance  $r$  from the center of the sphere, the potential is written in the form,

$$v_{\text{ext}}(\mathbf{r}, t) = v_{\text{ext}}(r, \infty) \left( 1 - e^{-t/\tau} \right), \quad (9)$$

$$v_{\text{ext}}(r, \infty) = \begin{cases} -V_0, & r \leq a_0, \\ 0, & a_0 < r \leq R. \end{cases} \quad (10)$$

We elucidate how the magnitude of the time constant  $\tau$  affects the dynamics of the particles.

### One-particle case

We start with the case of one particle ( $N = 1$ ). Suppose that the particle is initially in the  $n = 1$  state. Equations (2a) and (2b) are solved with the initial condition,

$$f_{k\sigma}(0) = \begin{cases} 1 & \text{for } k = \pi/R, \sigma = \uparrow, \\ 0 & \text{otherwise.} \end{cases} \quad (11)$$

Throughout this section, we set  $R/a_0 = 20$  and the upper limit of  $k$  is truncated at  $n = 60$ . The characteristic units of length and energy are  $a_0$  and  $\hbar^2 / 2ma_0^2$ , respectively. Accordingly, we introduce dimensionless energies  $\tilde{V}_0 \equiv 2ma_0^2 V_0 / \hbar^2$ ,  $\tilde{E}_{\text{tot}} \equiv 2ma_0^2 E_{\text{tot}} / \hbar^2$ , and

dimensionless times  $\tilde{t} \equiv \hbar t / 2ma_0^2$ ,  $\tilde{\tau} \equiv \hbar \tau / 2ma_0^2$ . The midpoint method has been employed for numerical integrations, where the time step between the midpoint and the next point is 0.01 in the above unit.

Figure 1 displays the time evolutions of the total energy for  $\tilde{V}_0 = 3$ . In the case  $\tilde{\tau} = 200$ ,  $\tilde{E}_{\text{tot}}$  gradually decreases and asymptotically approaches the exact ground-state energy<sup>[16]</sup> in the square-well potential,  $\tilde{\varepsilon}_1 = -0.0615$ , corroborating the adiabatic theorem. This case corresponds to the adiabatic regime,  $\omega_{21}\tau \gg 1$ , with  $\hbar\omega_{21} \equiv \varepsilon_{2\pi/R,\uparrow}^{(0)} - \varepsilon_{\pi/R,\uparrow}^{(0)}$  denoting the energy difference between  $n=1$  and  $n=2$  states. For  $\tilde{\tau} = 20$  ( $\omega_{21}\tau \approx 1$ ) or  $\tilde{\tau} = 2$  ( $\omega_{21}\tau < 1$ ), which corresponds to the nonadiabatic regime, the total energy in the final state is significantly higher than  $\tilde{\varepsilon}_1$ , indicating a breakdown of the adiabatic theorem.

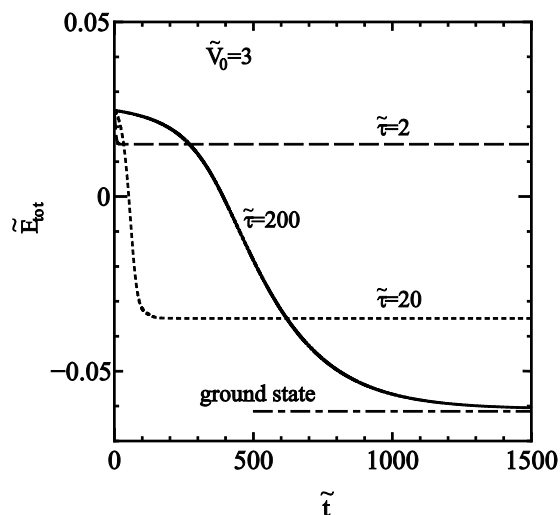


Figure 1. Time evolutions of the total energy in adiabatic (solid curve) and nonadiabatic cases (dashed and dotted curves).

The local particle density for spin  $\sigma$  at position  $\mathbf{r}$  can be expressed as

$$n_{\sigma}(r, t) = \sum_{kk'} \psi_{k\sigma}^{(0)*}(r) \psi_{k'\sigma}^{(0)}(r) \langle \rho_{kk'\sigma}(t) \rangle. \quad (12)$$

It can be found in Figure 2 that the computed density distribution  $n(r, t) = n_{\uparrow}(r, t)$  for  $\tilde{\tau} = 200$  converges to the exact ground-state value<sup>[16]</sup> already at  $\tilde{t} = 1500$ . The induced density calculated with the second-order perturbation theory, Eqs. (A3) and (A4) in Appendix, turns out too small, indicating a significance of the nonperturbative effect described by the nonlinear term in Eq. (2b).

In the final state,  $f_{k\sigma}$  is typically populated over a wide range in  $k$ -space, because a localized wave function is expressed by a linear combination of a large number of extended wave functions.

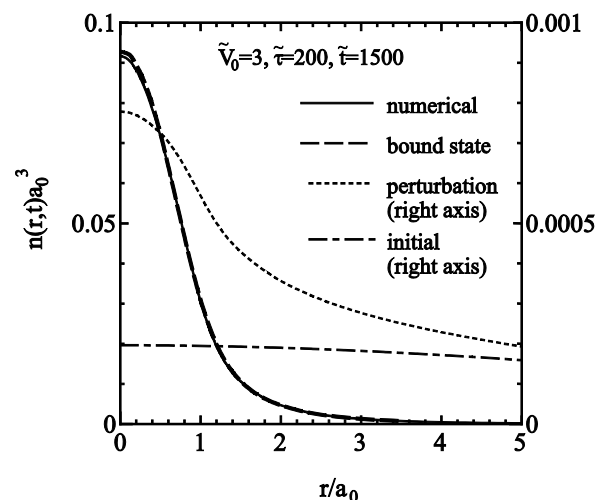


Figure 2. Density distributions at  $\tilde{t} = 1500$  evaluated with Eq. (12) in the case of an adiabatic switching ( $\tilde{V}_0 = 3$ ,  $\tilde{\tau} = 200$ ). The solid curve depicts the numerical solutions to Eqs. (2a) and (2b); the dashed curve is obtained through the ground-state wave function in the square-well potential.<sup>[16]</sup> The dotted and dot-dashed curves represent the second-order perturbation theory [Eqs. (A3) and (A4)] and the initial distribution, respectively, whose scale is given on the right axis.

Figure 3 compares time evolutions of the particle density at  $r=0$  for various combinations of  $\tilde{V}_0$  and  $\tilde{\tau}$ . A strong oscillation is observed after a nonadiabatic switching ( $\tilde{\tau} = 20$ ) of a strong potential ( $\tilde{V}_0 = 3$ ). For a nearly adiabatic switching ( $\tilde{\tau} = 100$ ), the amplitude of the oscillation is significantly reduced, but the oscillation period remains the same so far as  $\tilde{V}_0$  is fixed. For a weaker potential ( $\tilde{V}_0 = 2$ ), the amplitude gets smaller, the period becomes longer, and the shape is slightly distorted.

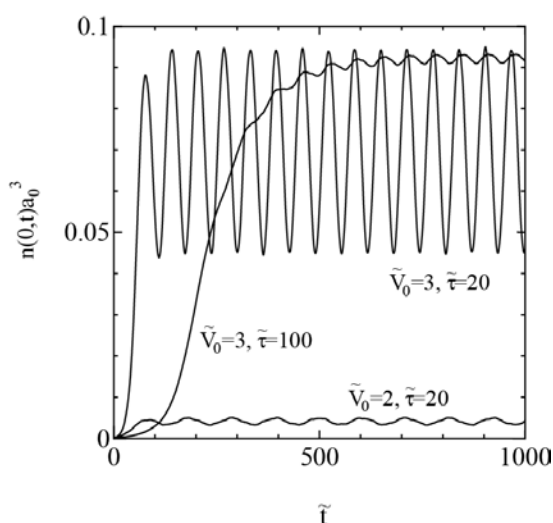


Figure 3. Time evolutions of  $n(0,t)$  for various combinations of  $\tilde{V}_0$  and  $\tilde{\tau}$ .

These oscillations can be interpreted as follows. In Figure 4, we plot the energy levels of the three lowest adiabatic states,  $\tilde{\epsilon}_n$  ( $n = 1, 2, 3$ ), as a function of the potential depth  $\tilde{V}$ , which can be obtained through solutions of the stationary-state Schrödinger equation in the usual way.<sup>[17]</sup> When  $\tilde{V}$  exceeds the threshold value  $\tilde{V}_{\text{th}} \equiv 2.468$ , the lowest level ( $n=1$ ) becomes a localized bound state and its energy is separated significantly from that of the delocalized excited state ( $n=2$ ). Oppositely, in the limit of  $\tilde{V} \rightarrow 0$ , the  $n=2$  state is slightly

more localized than  $n=1$ , since  $|\psi_{2\pi/R,\uparrow}^{(0)}(0)| > |\psi_{\pi/R,\uparrow}^{(0)}(0)|$  in Eq. (8). The characters of the two states are thus interchanged near  $\tilde{V} \approx \tilde{V}_{\text{th}}$ , where the energy separation between the two states is the smallest. Hence, the point  $\tilde{V} = \tilde{V}_{\text{th}}$  may be regarded as the Landau-Zener type crossing point.<sup>[7]</sup>

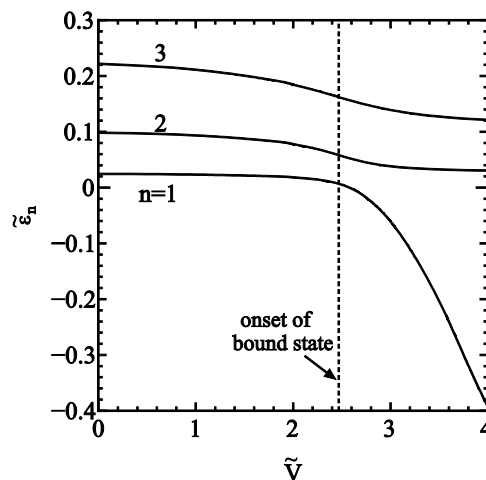


Figure 4. Energy levels of low-lying adiabatic states as a function of the potential depth.<sup>[17]</sup>

When the particle is initially in the  $n=1$  state and the potential  $\tilde{V}$  is switched on quickly from 0 to  $\tilde{V}_0$  across  $\tilde{V}_{\text{th}}$ , a nonadiabatic transition from  $n=1$  to  $n=2$  state may occur efficiently near  $\tilde{V} = \tilde{V}_{\text{th}}$ . Then, the wave function for  $t \gg \tau$  may be nonstationary and expressed as a superposition of those two states,

$$\psi(r,t) \approx a_1 e^{-i\tilde{\epsilon}_1 t} \psi_1(r) + a_2 e^{-i\tilde{\epsilon}_2 t} \psi_2(r), \quad (13)$$

where  $\psi_1(r)$  and  $\psi_2(r)$  are the corresponding stationary eigenfunctions, and the coefficients satisfy the relation  $|a_1|^2 + |a_2|^2 = 1$ . The total energy is then given as

$$\tilde{E}_{\text{tot}} = |a_1|^2 \tilde{\epsilon}_1 + |a_2|^2 \tilde{\epsilon}_2, \quad (14)$$

which is independent of time for  $t \gg \tau$ , as indicated in Figure 1. The density distribution

$n(r,t) = |\psi(r,t)|^2$  is likewise expressed as

$$n(r,t) = |a_1|^2 |\psi_1(r)|^2 + |a_2|^2 |\psi_2(r)|^2 + 2\text{Re} a_1^* a_2 \exp[-i(\tilde{\epsilon}_2 - \tilde{\epsilon}_1)\tilde{t}] \psi_1^*(r) \psi_2(r). \quad (15)$$

The last term on the right-hand side of Eq. (15) clearly manifests an oscillation, whose frequency  $\tilde{\epsilon}_2 - \tilde{\epsilon}_1$  depends strongly on  $V_0$  but is independent of  $\tau$ , accounting for the basic features shown in Figure 3.

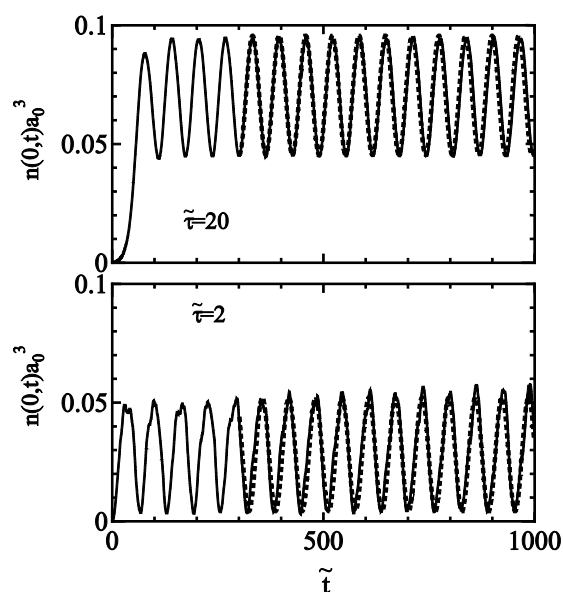


Figure 5. Density oscillations for  $\tilde{V}_0 = 3$ . The upper and lower panels correspond to the cases  $\tilde{\tau} = 20$  and  $\tilde{\tau} = 2$ , respectively. The solid curves depict numerical solutions to Eqs. (2a) and (2b); the dotted curves refer to the two-state picture, Eq. (15).

Based on this two-state picture, we have analyzed the data for  $\tilde{V}_0 = 3$  quantitatively. We note that, since  $\psi_1(r)$  and  $\psi_2(r)$  are real, the coefficients  $a_1$  and  $a_2$  can be taken as real and positive; such a restriction merely brings an

unimportant phase factor to the exponential factor in Eq. (15). By using Eq. (14) in conjunction with the computed values of  $\tilde{E}_{\text{tot}}$  displayed in Figure 1, we obtain  $a_1 = 0.856$  and  $a_2 = 0.517$  for  $\tilde{\tau} = 20$ ;  $a_1 = 0.482$  and  $a_2 = 0.876$  for  $\tilde{\tau} = 2$ . These values are then substituted into Eq. (15) to compute  $n(0,t)$ .

The results are shown in Figure 5. We find that, once the phase factor is chosen appropriately, the two-state picture can excellently reproduce the oscillatory behaviors. The time-averaged value of  $n(0,t)$  for  $\tilde{\tau} = 2$  turns out smaller than that for  $\tilde{\tau} = 20$ , because a faster switching leads to a larger population of the  $n=2$  state which is more delocalized than the  $n=1$  state. In case  $\tilde{V}_0 < \tilde{V}_{\text{th}}$ , the nonadiabatic transition is not triggered and hence the oscillatory feature is significantly weak, which is consistent with the case  $\tilde{V}_0 = 2$  in Figure 3.

We mention that, in a nonadiabatic excitation of a BCS superconductor, an oscillation of the order parameter was likewise observed<sup>[3,4]</sup> and its origin was identified as a coherent superposition of different quasiparticle states.<sup>[4]</sup>

Another familiar example of an oscillation between two quantum states is the Rabi oscillation in an atom interacting with a coherent laser field.<sup>[18]</sup> It can be derived from Eqs. (2a) and (2b) when they are applied to a two-level system.<sup>[18]</sup> We also mention that a method combining the Floquet theory and the density-matrix equation has been proposed to analyze nonlinear optical processes in two-level atoms.<sup>[19]</sup>

### Ideal Fermi Gas

We then proceed to the case of a Fermi gas consisting of  $N$  noninteracting particles. The initial condition for  $f_{k\sigma}(0)$  is now given by the Fermi distribution,

$$f_{k\uparrow}(0) = f_{k\downarrow}(0) = \begin{cases} 1, & \text{for } k \leq k_F, \\ 0, & \text{otherwise.} \end{cases} \quad (16)$$

The Fermi wave number  $k_F$  is fixed at  $k_F = \pi/4a_0$  throughout this section. We consider only  $s$ -waves for simplicity; the relation between  $N$  and  $k_F$  is given by  $N = 2Rk_F/\pi$ .

Time evolutions of  $n(0,t) \equiv n_{\uparrow}(0,t) + n_{\downarrow}(0,t)$  are compared in Figure 6 for various combinations of  $R$  and  $\tilde{\tau}$  in the case of  $\tilde{V}_0 = 3$ . It can be found that the shape of the nonadiabatic oscillation for  $R/a_0=20$  and  $\tilde{\tau}=20$  is rather irregular and its amplitude is small compared with the corresponding result (Figure 5) for one particle. In the Fermi gas, the nonadiabatic transition from  $n=1$  to  $n=2$  state in Figure 4 is hindered because the  $n=2$  state is already occupied (i.e., Pauli blocking). The irregular oscillation in Figure 6 may therefore be considered as a superposition of many weak transitions to unoccupied states across the Fermi level, each having a different oscillation frequency. As the system size  $R$  increases, the spacing between neighboring levels becomes narrow and the overall oscillatory behavior tends to be smeared out. The oscillation disappears for  $\tilde{\tau} = 100$ , indicating that the time evolution in this case is adiabatic.

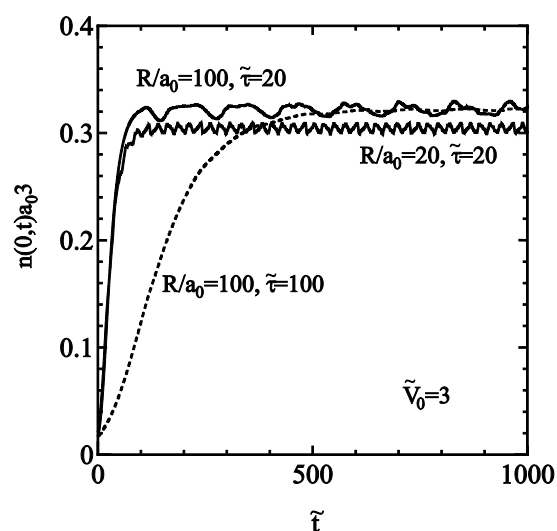


Figure 6. Time evolutions of  $n(0,t)$  for  $\tilde{V}_0 = 3$ .

Our simulation for an adiabatic case converges automatically to an equilibrium state. Let us examine whether the distributions of metallic electrons around a static impurity can be reproduced in this way. Friedel showed that the induced electron distribution at distance  $r$  far from the impurity can generally be expressed, up to the  $1/r^4$  term, as<sup>[14,16,20]</sup>

$$\Delta n(r) \approx -\frac{1}{2\pi^2 r^3} \sum_{l=0}^{\infty} (2l+1) \sin \delta_l(k_F) \times \left\{ \cos[2k_F r + \delta_l(k_F) - l\pi] - \frac{\sin[2k_F r + \delta_l(k_F) - l\pi]}{2k_F r} \right\}. \quad (17)$$

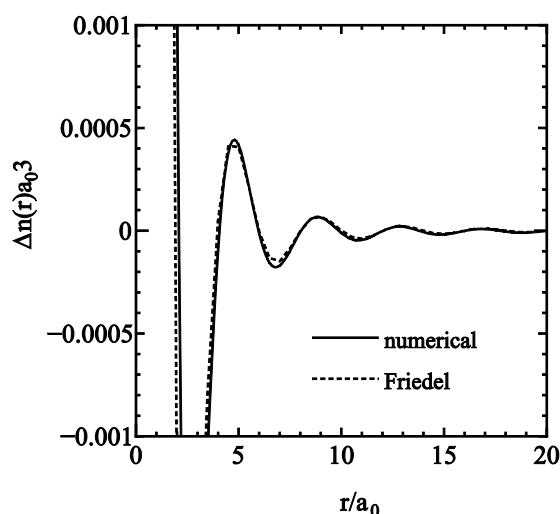


Figure 7. Induced density at  $\tilde{\tau} = 1000$  for  $R/a_0 = 100$ ,  $\tilde{V}_0 = 3$  and  $\tilde{\tau} = 100$  (solid curve), compared with the  $l = 0$  term in Eq. (17) (dotted curve).

Here,  $\delta_l(k_F)$  is the scattering phase shift for a partial wave with angular momentum  $l$  and wave number  $k_F$ . For  $s$ -wave ( $l = 0$ ), it can be evaluated as<sup>[16]</sup>

$$\delta_0(k_F) = \tan^{-1} \left[ \left( \frac{k_F}{k_s} \right) \tan(k_s a_0) \right] - k_F a_0 \quad (18)$$

with  $k_s a_0 = [\tilde{V}_0 + (k_F a_0)^2]^{1/2}$ . Equation (17) exhibits an oscillatory behavior, known as the Friedel oscillation, arising from the discontinuity in the Fermi distribution at  $k = k_F$ . In our simulation,  $\Delta n(r)$  can be evaluated in accordance with  $\Delta n(r) = n(r, \infty) - n(r, 0)$ . Figure 7 reveals that our simulation result for  $R/a_0 = 100$  can reproduce the  $l=0$  part of the Friedel oscillation accurately.

Generally, when an electron gas is perturbed by a local potential, the electrons are scattered out of the Fermi sea,<sup>[13,14]</sup> causing a rounding of the Fermi distribution. Such a feature can be confirmed through the solid curve in Figure 8, which illustrates a typical momentum distribution function obtained through Eqs. (2a) and (2b) after an adiabatic switching.

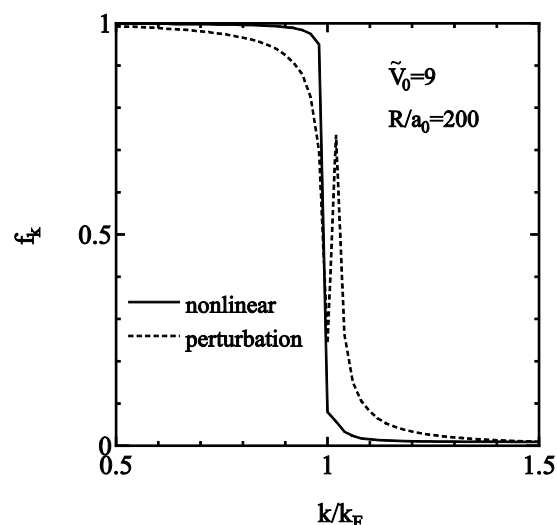


Figure 8. Momentum distribution functions  $f_k \equiv f_{k\uparrow} = f_{k\downarrow}$  for  $R/a_0 = 200$ ,  $\tilde{V}_0 = 9$  and  $\tilde{\tau} = 300$ , computed at  $\tilde{t} = 1500$ . The solid curve represents the full solutions to Eqs. (2a) and (2b); the dotted curve is evaluated by the perturbation formulas (A1) and (A4).

It would be instructive to compare the result with the perturbation theory. Formula (A4) can be evaluated in the bulk limit  $R \rightarrow \infty$  as

$$f_{k\sigma}^{(2)}(\infty) = -\frac{\tilde{V}_0^2 a_0}{\pi R} I(k a_0), \quad (19)$$

with

$$I(x) = \int_{(k_F + \pi/R)a_0}^{\infty} dx' \frac{1}{(x' - x)^2 (x' + x)^2} \times \left[ \frac{\sin(x' - x)}{x' - x} - \frac{\sin(x' + x)}{x' + x} \right]^2. \quad (20)$$

This integral is divergent for  $x \rightarrow k_F a_0$  and  $R \rightarrow \infty$ . A reasonably accurate analytic formula that reproduces Eq. (20) for  $0 < x < k_F a_0$  is

$$I(x) \approx \frac{1}{(2k_F a_0)^2} \left[ 1 - \frac{\sin(2k_F a_0)}{2k_F a_0} \right]^2 \times \left[ \frac{1}{(k_F + \frac{\pi}{R})a_0 - x} - \frac{1}{k_F a_0} \right]. \quad (21)$$

Equation (19), combined with Eq. (21), can lead to an unphysical behavior such that  $f_{k\sigma} < 0$  ( $k \rightarrow k_F - 0$ ) and  $f_{k\sigma} > 1$  ( $k \rightarrow k_F + 0$ ) when  $\tilde{V}_0$  is large. Even for a finite-size system, such an anomaly is exposed by two sharp peaks below and above  $k_F$ , as indicated by the dotted curve in Figure 8. When the nonperturbative effect is fully taken into account (solid curve), the unphysical feature no longer appears even though the potential is fairly strong ( $\tilde{V}_0 = 9$ ).

These low-energy excitations give rise to the infrared (or orthogonalization) catastrophe predicted by Anderson.<sup>[12-14]</sup> He proved for a system of noninteracting Fermions that the many-body wave function (i.e., the Slater determinant) in the presence of a local potential becomes orthogonal to that in the

absence of the potential as the system size increases; namely, the overlap integral  $S$  of the two Slater determinants vanishes<sup>[12]</sup> as  $N^{-\varepsilon}$ ,  $\varepsilon > 0$ . The infrared catastrophe is responsible for anomalies in the x-ray absorption or photoemission spectra.<sup>[2]</sup>

Let us revisit this problem through the density-matrix theory. When  $k$  and  $k'$  designate the occupied states below the Fermi level, the density matrix (1) can be regarded as a  $N/2$  by  $N/2$  matrix, which we denote shortly as  $\rho_{\sigma}(t)$ . Then, it follows that

$$S^2 = \left| \det \rho_{\uparrow}(\infty) \right| = \left| \det \rho_{\downarrow}(\infty) \right|, \quad (22)$$

provided that the adiabatic theorem is satisfied. Hence,  $S$  is directly accessible through our adiabatic simulations.

In addition, the perturbation theory of the density matrix yields an approximate analytic expression for  $S$  in the bulk limit, which has not been reported before. To derive such a formula, we employ Eqs. (A3) and (A4), taking the limits  $|\omega_{k'k\sigma}| \tau \gg 1$ ,  $t \gg \tau$ , and  $R \rightarrow \infty$ . It follows from Eqs. (16) and (A3) that  $\langle \rho_{kk'\sigma}(t) \rangle = 0$  if both  $k$  and  $k' (\neq k)$  are occupied states. Thus,

$$\begin{aligned} \det \rho_{\sigma}(\infty) &= \prod_{k \leq k_F} \left[ 1 + f_{k\sigma}^{(2)}(\infty) \right] \\ &\approx \exp \left[ \sum_{k \leq k_F} f_{k\sigma}^{(2)}(\infty) \right] \\ &\approx \exp \left[ \frac{R}{\pi} \int_0^{k_F} dk f_{k\sigma}^{(2)}(\infty) \right]. \end{aligned} \quad (23)$$

By substituting Eqs. (19) and (21) into Eq. (23) and carrying out the  $k$ -integration, we arrive at

$$S^2 = \left( \frac{N}{2} \right)^{-C}, \quad (24)$$

$$C \approx \left( \frac{\tilde{V}_0}{2\pi k_F a_0} \right)^2 \left[ 1 - \frac{\sin(2k_F a_0)}{2k_F a_0} \right]^2. \quad (25a)$$

In particular, for a weak potential such that  $\tilde{V}_0 \ll (k_F a_0)^2$ , the comparison between Eqs. (18) and (25) yields

$$C \approx [\delta_0(k_F) / \pi]^2, \quad (25b)$$

an analytic expression often seen in the literature.<sup>[14]</sup>

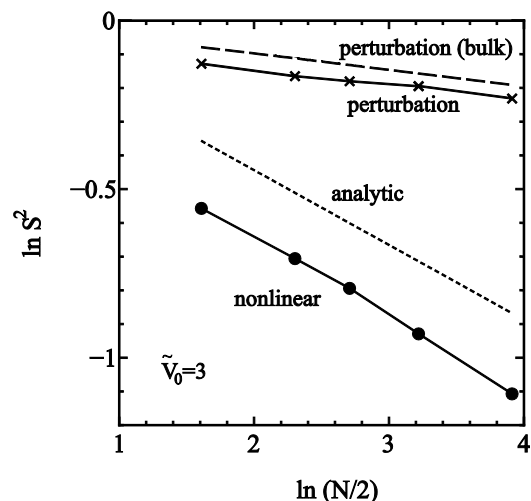


Figure 9. The Anderson's overlap integral for  $\tilde{V}_0 = 3$  calculated with Eq. (22). The dots are obtained through full solutions of Eqs. (2a) and (2b); the crosses are the perturbation-theoretic results based on Eqs. (A3) and (A4). The solid lines are for a guide to the eyes. The dashed and dotted curves depict formulas (25a) and (25b), respectively, combined with Eq. (24).

Figure 9 compares the behaviors of  $S^2$  for  $\tilde{V}_0 = 3$  obtained by different methods. Within the perturbation theory, the numerical results

for finite-size systems agree fairly well with the bulk formula (25a), although a discrepancy exists due to the smallness of  $N$  ( $N = 10-100$ ). In the original article,<sup>[12]</sup> Anderson provided only an upper bound of  $S$  by neglecting the enhanced particle density inside the potential well. Figure 9 reveals that the nonperturbative effect, described by the nonlinear term in Eq. (2b), reduces the values of  $S$  significantly. The slope of the curve turns out to be consistent with formula (25b) rather than (25a), although both formulas are derived through perturbation theories. The largest system size treated in the simulation is  $R/a_0 = 200$ , where energy levels up to  $n = 360$  have been included in Eq. (8).

Although the oscillation in the nonadiabatic regime is suppressed by Pauli blocking in noninteracting Fermi gas, it would emerge as the plasma oscillation in interacting electron gas.<sup>[14]</sup> The plasma oscillation stems from the self-energy matrix (4). The contributions from the states with higher angular-momentum quantum numbers ( $p$ -,  $d$ -waves, etc.) should also be considered in order for a realistic description of the energy levels and dynamics of three-dimensional Fermi gas. These are the issues for future studies.

## Multiphoton ionization

We shall prove in this section that the nonlinear term in Eq. (2b) can account for the Keldysh formula of multiphoton ionization.<sup>[5,6]</sup> We consider the ionization of a  $1s$  electron in a hydrogen-like atom by an oscillating electric field  $\mathbf{E}(t) = E_0 \cos(\omega t)$ . The potential of external field is written as  $v_{\text{ext}}(\mathbf{r}, t) = e\mathbf{r} \cdot \mathbf{E}(t)$ , with  $e$  denoting the elemental charge. The spin index is neglected for brevity.

The underlying assumptions in the Keldysh theory are: (i) the bound states other than  $1s$  are neglected; and (ii) the continuum wave functions are approximated by the plane waves  $\psi_{\mathbf{k}}^{(0)}(\mathbf{r}) = e^{i\mathbf{k} \cdot \mathbf{r}} / \sqrt{\Omega}$ , with  $\Omega$  denoting the volume of the system. Equation (2b) can then be expressed as

$$i\hbar \frac{\partial \langle \rho_{\mathbf{k},1s}(t) \rangle}{\partial t} = -(\varepsilon_{\mathbf{k}}^{(0)} - \varepsilon_{1s}^{(0)}) \langle \rho_{\mathbf{k},1s}(t) \rangle - \mathbf{d}_{1s,\mathbf{k}} \cdot \mathbf{E}(t) [f_{\mathbf{k}}(t) - f_{1s}(t)] + \sum_{\mathbf{k}'(\neq \mathbf{k})} \mathbf{d}_{\mathbf{k}'\mathbf{k}} \cdot \mathbf{E}(t) \langle \rho_{\mathbf{k}',1s}(t) \rangle, \quad (26)$$

where

$$\mathbf{d}_{1s,\mathbf{k}} \equiv \int d\mathbf{r} \psi_{1s}^{(0)*}(\mathbf{r})(-e)\mathbf{r} \psi_{\mathbf{k}}^{(0)}(\mathbf{r}) = \mathbf{d}_{\mathbf{k},1s}^*, \quad (27)$$

$$\mathbf{d}_{\mathbf{k}'\mathbf{k}} \equiv \int d\mathbf{r} \psi_{\mathbf{k}'}^{(0)*}(\mathbf{r})(-e)\mathbf{r} \psi_{\mathbf{k}}^{(0)}(\mathbf{r}) = \frac{-e}{i\Omega} (2\pi)^3 \frac{\partial}{\partial \mathbf{k}} \delta(\mathbf{k}' - \mathbf{k}) \quad (28)$$

refer to the dipole transition matrix elements.

With the help of Eq. (28), the last term on the right-hand side of Eq. (26), i.e., the nonperturbative term, can be rewritten as  $i e \mathbf{E}(t) \cdot \partial \langle \rho_{\mathbf{k},1s}(t) \rangle / \partial \mathbf{k}$ . To proceed further, we make the transformation  $\{t, \mathbf{k}\} \rightarrow \{\tilde{t}, \tilde{\mathbf{k}}\}$  according to  $\tilde{t} = t$ ,  $\tilde{\mathbf{k}} = \mathbf{k} + \frac{e}{\hbar} \int_0^{\tilde{t}} dt' \mathbf{E}(t')$   $\equiv \mathbf{k} + \boldsymbol{\eta}(\tilde{t})$ .<sup>[21]</sup> Equation (26) is then transformed as

$$\frac{\partial \langle \rho_{\tilde{\mathbf{k}}-\boldsymbol{\eta}(\tilde{t}),1s}(\tilde{t}) \rangle}{\partial \tilde{t}} = i \frac{\varepsilon_{\tilde{\mathbf{k}}-\boldsymbol{\eta}(\tilde{t})}^{(0)} - \varepsilon_{1s}^{(0)}}{\hbar} \langle \rho_{\tilde{\mathbf{k}}-\boldsymbol{\eta}(\tilde{t}),1s}(\tilde{t}) \rangle + \frac{i}{\hbar} \mathbf{d}_{1s,\tilde{\mathbf{k}}-\boldsymbol{\eta}(\tilde{t})} \cdot \mathbf{E}(\tilde{t}) [f_{\tilde{\mathbf{k}}-\boldsymbol{\eta}(\tilde{t})}(\tilde{t}) - f_{1s}(\tilde{t})]. \quad (29)$$

We further approximate as  $f_{\tilde{\mathbf{k}}-\boldsymbol{\eta}(\tilde{t})}(\tilde{t}) \approx 0$  and  $f_{1s}(\tilde{t}) \approx 1$  by neglecting the saturation effect. Equation (29) can then be integrated easily and transformed back to the  $\{t, \mathbf{k}\}$  representation as

$$\langle \rho_{\mathbf{k},1s}(t) \rangle \approx -\frac{i}{\hbar} \int_0^t ds \mathbf{d}_{1s,\mathbf{k}+\boldsymbol{\eta}(t)-\boldsymbol{\eta}(s)} \cdot \mathbf{E}(s) \times \exp \left[ i \int_s^t dt' \frac{\varepsilon_{\mathbf{k}+\boldsymbol{\eta}(t)-\boldsymbol{\eta}(t')} - \varepsilon_{1s}^{(0)}}{\hbar} \right]. \quad (30)$$

On the other hand, Eq. (2a) can be rewritten as

$$\frac{\partial f_{\mathbf{k}}(t)}{\partial t} = -\frac{2}{\hbar} \text{Im} \mathbf{d}_{\mathbf{k},1s} \cdot \mathbf{E}(t) \langle \rho_{\mathbf{k},1s}(t) \rangle. \quad (31)$$

By substituting Eq. (30) into Eq. (31), the ionization rate can be evaluated in accordance with  $w = \lim_{t \rightarrow \infty} \sum_{\mathbf{k}} \partial f_{\mathbf{k}}(t) / \partial t$ . By assuming the free-electron spectrum  $\varepsilon_{\mathbf{k}}^{(0)} = \hbar^2 k^2 / 2m$ , the result is

$$w = \frac{2}{\hbar^2} \lim_{t \rightarrow \infty} \text{Re} \sum_{\mathbf{k}} L^*(\mathbf{k}, t) \cos(\omega t) \times \int_0^t ds L(\mathbf{k}, s) \cos(\omega s), \quad (32)$$

with

$$L(\mathbf{k}, s) \equiv \exp \left( \frac{i e \mathbf{E}_0 \cdot \mathbf{k}}{m \omega^2} \right) \times \exp \left[ -\frac{i}{\hbar} \left( \frac{\hbar^2 k^2}{2m} - \varepsilon_{1s}^{(0)} + \frac{e^2 E_0^2}{4m \omega^2} \right) s \right] \times V_0 \left( \mathbf{k} - \frac{e \mathbf{E}_0}{\hbar \omega} \sin(\omega s) \right) \times \exp \left[ -\frac{i e \mathbf{E}_0 \cdot \mathbf{k}}{m \omega^2} \cos(\omega s) + \frac{e^2 E_0^2}{8m \hbar \omega^3} \sin(2\omega s) \right], \quad (33)$$

and  $V_0(\mathbf{k}) \equiv \mathbf{d}_{1s,\mathbf{k}} \cdot \mathbf{E}_0$ . Equation (32) is equivalent to Eq. (8) of the original article by Keldysh,<sup>[5]</sup> except for a presence of the factor 2 in the former. The product of the last two factors on the right-hand side of Eq. (33) is a periodic function of  $\omega s$ , so that it can be

expanded in a Fourier series.<sup>[5]</sup> We thus reproduce the Keldysh formula,

$$w = \frac{2\pi}{\hbar} \sum_{\mathbf{k}} \sum_{n=0}^{\infty} |L(\mathbf{k})|^2 \times \delta \left( \frac{\hbar^2 k^2}{2m} + U_p - \varepsilon_{1s}^{(0)} - n \hbar \omega \right), \quad (34)$$

where

$$L(\mathbf{k}) \equiv \frac{1}{2\pi} \int_{-\pi}^{\pi} dx \cos x V_0 \left( \mathbf{k} - \frac{e \mathbf{E}_0}{\hbar \omega} \sin x \right) \times \exp \left[ -i \left( \frac{e \mathbf{E}_0 \cdot \mathbf{k}}{m \omega^2} \cos x - \frac{e^2 E_0^2}{8m \hbar \omega^3} \sin(2x) \right) \right] \times \exp \left[ -i \frac{x}{\hbar \omega} \left( \frac{\hbar^2 k^2}{2m} - \varepsilon_{1s}^{(0)} + \frac{e^2 E_0^2}{4m \omega^2} \right) \right], \quad (35)$$

and  $U_p \equiv e^2 E_0^2 / 4m \omega^2$  refers to the ponderomotive energy.<sup>[5,6]</sup> Equation (34) manifests the  $n$ -photon process under the ponderomotive shift at high intensities, called as the above-threshold ionization.<sup>[6]</sup>

## Conclusions

We have presented density matrix equations describing the quantum dynamics in the TDUHF approximation, where the nonperturbative effect due to the time-dependent external field is incorporated through the nonlinear term. With the knowledge of the UHF wave functions in the initial unperturbed state, subsequent time evolutions of total energies, particle densities and so forth, can be computed through numerical integrations of the density matrix equations.

We have thereby analyzed the dynamics of ideal Fermi gas around a square-well potential switched on with an arbitrary time constant  $\tau$ . When  $\tau$  is small, an oscillation of a particle

stems from a quantum superposition of  $n=1$  and  $n=2$  states driven by a nonadiabatic transition at the Landau-Zener type crossing point. The oscillation is clearly seen when the system size  $N$  is small but smeared out by the Pauli blocking effect as  $N$  increases.

In the case of a slow switching for which the adiabatic theorem holds, our simulations have successfully reproduced the long-range Friedel oscillation characteristic of an electron gas around an impurity atom. We have shown that the strong localization of a particle inside the potential well tends to enhance the Anderson's infrared catastrophe significantly.

We have also presented a straightforward derivation of the Keldysh formula of atomic multiphoton ionization through the density-matrix formalism. The present theory is thus applicable to various types of nonadiabatic perturbations; it would provide a basis for analyzing ultrafast electron dynamics under intense x-rays, for example.

It has been known that a confined Fermi gas exhibits a shell structure,<sup>[22]</sup> whose influence on the infrared catastrophe was recently discussed by Bandopadhyay and Hentschel.<sup>[23]</sup> It would be an interesting issue to analyze the quantum dynamics of interacting particles confined in various mesoscopic geometries.<sup>[24]</sup> In doing so, the interaction between electrons can be incorporated through the self-energy matrix (4).

## Acknowledgments

The author would like to thank Dr. A. Ichimura for pertinent discussions. This work was supported in part through Grant-in-Aid for Scientific Research (A) provided by JSPS.

## Appendix. Perturbation theory

General properties of perturbative solutions to the time-dependent Schrödinger equation for various types of external fields were discussed in detail by Langhoff *et al.*<sup>[25]</sup> with the wavefunction formalism, and by Hammer and Weber<sup>[26]</sup> with the  $U$ -matrix approach. Here, we present perturbative solutions to the density matrix equations (2a) and (2b) in compact analytical forms for the case of noninteracting particles.

When the external field (9) is weak, the diagonal and off-diagonal components of the density matrix can be expressed in a perturbation series as

$$f_{k\sigma}(t) = f_{k\sigma}^{(0)} + f_{k\sigma}^{(1)}(t) + f_{k\sigma}^{(2)}(t) + \dots, \\ \langle \rho_{kk'\sigma}(t) \rangle = \langle \rho_{kk'\sigma}^{(1)}(t) \rangle + \dots, \quad k \neq k', \quad (\text{A1})$$

with the initial conditions  $f_{k\sigma}(0) = f_{k\sigma}^{(0)}$  and  $\langle \rho_{kk'\sigma}(0) \rangle = 0$ . The first-order solution to equation (2b) is determined through

$$i\hbar \frac{\partial \langle \rho_{kk'\sigma}^{(1)}(t) \rangle}{\partial t} = (\varepsilon_{k'\sigma}^{(0)} - \varepsilon_{k\sigma}^{(0)}) \langle \rho_{kk'\sigma}^{(1)}(t) \rangle \\ + (v_{\text{ext}}(\infty))_{k'k\sigma} (1 - e^{-t/\tau}) (f_{k\sigma}^{(0)} - f_{k'\sigma}^{(0)}). \quad (\text{A2})$$

Analytic solution to this equation can be expressed in terms of the energy difference

$$\hbar\omega_{k'k\sigma} = \varepsilon_{k'\sigma}^{(0)} - \varepsilon_{k\sigma}^{(0)} \quad \text{as}$$

$$\langle \rho_{kk'\sigma}^{(1)}(t) \rangle = -\frac{(v_{\text{ext}}(\infty))_{k'k\sigma}}{\hbar} (f_{k\sigma}^{(0)} - f_{k'\sigma}^{(0)}) \\ \times \left[ \frac{1 - e^{-i\omega_{k'k\sigma}t}}{\omega_{k'k\sigma}} - \frac{e^{-t/\tau} - e^{-i\omega_{k'k\sigma}t}}{\omega_{k'k\sigma} + \frac{i}{\tau}} \right]$$

$$\approx \begin{cases} -\frac{(v_{\text{ext}}(\infty))_{k'k\sigma}}{\hbar} (f_{k\sigma}^{(0)} - f_{k'\sigma}^{(0)}) \frac{1 - e^{-t/\tau}}{\omega_{k'k\sigma}}, \\ \text{for } |\omega_{k'k\sigma}| \tau \gg 1, \\ -\frac{(v_{\text{ext}}(\infty))_{k'k\sigma}}{\hbar} (f_{k\sigma}^{(0)} - f_{k'\sigma}^{(0)}) \frac{1 - e^{-i\omega_{k'k\sigma}t}}{\omega_{k'k\sigma}}, \\ \text{for } |\omega_{k'k\sigma}| \tau \ll 1. \end{cases} \quad (\text{A3})$$

This solution is substituted into Eq. (2a), leading to

$$\begin{aligned} f_{k\sigma}^{(1)}(t) &= 0, \\ f_{k\sigma}^{(2)}(t) &= -\frac{2}{\hbar^2} \sum_{k'(\neq k)} |(v_{\text{ext}}(\infty))_{k'k\sigma}|^2 (f_{k\sigma}^{(0)} - f_{k'\sigma}^{(0)}) \\ &\quad \times \left\{ \left[ \frac{1}{\omega_{k'k\sigma}^2 + \frac{1}{\tau^2}} - \frac{1}{\omega_{k'k\sigma}^2} \right] [\cos(\omega_{k'k\sigma}t) - 1] \right. \\ &\quad - \frac{\sin(\omega_{k'k\sigma}t)}{\omega_{k'k\sigma}\tau \left( \omega_{k'k\sigma}^2 + \frac{1}{\tau^2} \right)} (1 - e^{-t/\tau}) \\ &\quad \left. + \frac{1}{\omega_{k'k\sigma}^2 + \frac{1}{\tau^2}} \frac{1}{2} (1 - e^{-t/\tau})^2 \right\} \\ &\approx \begin{cases} -\frac{1}{\hbar^2} \sum_{k'(\neq k)} |(v_{\text{ext}}(\infty))_{k'k\sigma}|^2 \frac{f_{k\sigma}^{(0)} - f_{k'\sigma}^{(0)}}{\omega_{k'k\sigma}^2} (1 - e^{-t/\tau})^2, \\ \text{for } |\omega_{k'k\sigma}| \tau \gg 1, \\ -\frac{2}{\hbar^2} \sum_{k'(\neq k)} |(v_{\text{ext}}(\infty))_{k'k\sigma}|^2 \frac{f_{k\sigma}^{(0)} - f_{k'\sigma}^{(0)}}{\omega_{k'k\sigma}^2} \\ \times [1 - \cos(\omega_{k'k\sigma}t)], \text{ for } |\omega_{k'k\sigma}| \tau \ll 1. \end{cases} \end{aligned} \quad (\text{A4})$$

Note that Eq. (A4) duly satisfies the particle-number conservation  $\sum_{k\sigma} f_{k\sigma}^{(2)}(t) = 0$ , but does not necessarily satisfy the constraint  $0 \leq f_{k\sigma}(t) \leq 1$  for Fermions.

In the nonadiabatic limit  $|\omega_{k'k\sigma}| \tau \ll 1$ , both Eqs. (A3) and (A4) contain oscillatory terms, whose frequency is equal to the energy difference between the two states. We note, however, that the coherent oscillation indicated in Figure 5 is basically a nonperturbative effect.

The total energy at time  $t$  can be calculated with Eqs. (6), (A3) and (A4) as

$$\begin{aligned} E_{\text{tot}}(t) &\approx \sum_{k\sigma} \left[ \varepsilon_{k\sigma}^{(0)} + (v_{\text{ext}}(\infty))_{kk\sigma} (1 - e^{-t/\tau}) \right] f_{k\sigma}^{(0)} \\ &\quad + \sum_{k\sigma} \sum_{k'(\neq k)} \frac{|(v_{\text{ext}}(\infty))_{k'k\sigma}|^2}{\hbar} f_{k\sigma}^{(0)} (1 - f_{k'\sigma}^{(0)}) \\ &\quad \times \left\{ -\frac{(1 - e^{-t/\tau})^2}{\omega_{k'k\sigma}} \right. \\ &\quad \left. + \frac{1 + e^{-2t/\tau} - 2e^{-t/\tau} \cos(\omega_{k'k\sigma}t)}{\tau^2 \omega_{k'k\sigma} \left( \omega_{k'k\sigma}^2 + \frac{1}{\tau^2} \right)} \right\}. \end{aligned} \quad (\text{A5})$$

Here, the first and the second terms inside the curly brackets represent the adiabatic and nonadiabatic components, respectively, of the second-order energy: These two terms were derived recently by Mandal and Hunt<sup>[27]</sup> in a more general form.

The asymptotic total energy is

$$E_{\text{tot}}(\infty) \approx \begin{cases} \left[ \sum_{k\sigma} \left[ \varepsilon_{k\sigma}^{(0)} + (v_{\text{ext}}(\infty))_{kk\sigma} \right. \right. \\ \left. \left. - \sum_{k'(\neq k)} \frac{|(v_{\text{ext}}(\infty))_{k'k\sigma}|^2}{\varepsilon_{k'\sigma}^{(0)} - \varepsilon_{k\sigma}^{(0)}} (1 - f_{k'\sigma}^{(0)}) \right] f_{k\sigma}^{(0)} \right] \\ \text{for } |\omega_{k'k\sigma}| \tau \gg 1, \\ \sum_{k\sigma} \left[ \varepsilon_{k\sigma}^{(0)} + (v_{\text{ext}}(\infty))_{kk\sigma} \right] f_{k\sigma}^{(0)}, \\ \text{for } |\omega_{k'k\sigma}| \tau \ll 1. \end{cases} \quad (\text{A6})$$

Here, the expression for the adiabatic limit  $|\omega_{k'k\sigma}| \tau \gg 1$  was derived earlier by McWeeny<sup>[28]</sup> through a stationary perturbation theory of the density matrix. It is interesting to note here that the second-order perturbation term in the expression for  $|\omega_{k'k\sigma}| \tau \gg 1$ , which stems from a modification of the wave function due to perturbation, is absent for a sufficiently fast switching,  $|\omega_{k'k\sigma}| \tau \ll 1$ .

**Keywords:** density matrix, nonadiabatic transition, infrared catastrophe, multiphoton ionization

## References and Notes

1. P. Schmüser, M. Dohlus, J. Rossbach, *Ultraviolet and Soft X-Ray Free-Electron Lasers*; Springer: Berlin, **2008**.
2. F. de Groot, A. Kotani, *Core Level Spectroscopy of Solids*; CRC Press: FL, **2008**, Chapter 3.
3. R. Matsunaga, Y.I. Hamada, K. Makise, Y. Uzawa, H. Terai, Z. Wang, R. Shimano, *Phys. Rev. Lett.* **2013**, 111, 057002.
4. T. Papenkort, V.M. Axt, T. Kuhn, *Phys. Rev. B* **2007**, 76, 224522.
5. L.V. Keldysh, *Sov. Phys. JETP* **1965**, 20, 1307.
6. M. Protopapas, C.H. Keitel, P.L. Knight, *Rep. Prog. Phys.* **1997**, 60, 389.
7. H. Nakamura, *Nonadiabatic Transition, 2nd ed.*; World Scientific: Singapore, **2012**, Chapter 2.
8. A. Messiah, *Quantum mechanics*; North-Holland: Amsterdam, **1962**, Chapter 17.
9. A.D. McLachlan, M.A. Ball, *Rev. Mod. Phys.* **1964**, 36, 844.
10. H. Kitamura, *J. Phys. B: At. Mol. Opt. Phys.* **2010**, 43, 115601.
11. R. McWeeny, *Methods of Molecular Quantum Mechanics*, 2nd ed.;
- Academic Press: London, **1996**, Chapters 11 and 12.
12. P.W. Anderson, *Phys. Rev. Lett.* **1967**, 18, 1049.
13. P.W. Anderson, in *The Hubbard Model*; D. Baeriswyl, D.K. Campbell, J.M.P. Carmelo, F. Guinea, E. Louis, Eds.; Plenum: NY, **1995**, p. 217.
14. K. Yamada, *Electron Correlation in Metals*; Cambridge Univ. Press: Cambridge, **2004**, Chapters 1 and 3.
15. C.A. Ullrich, *Time-Dependent Density-Functional Theory, Concepts and Applications*; Oxford: Croydon, **2012**, Chapter 9.
16. J.S. Galsin, *Impurity Scattering in Metallic Alloys*; Kluwer: NY, **2002**, Chapters 9 and 10.
17. Figure 5 can be obtained in another way: We perform adiabatic simulations starting from  $n=2$  and  $n=3$  initial states, and obtain  $E_{\text{tot}}-t$  relations similar to the solid curve in Figure 1 ( $n=1$ ). By virtue of the adiabatic theorem, the instantaneous value of  $\tilde{E}_{\text{tot}}$  at time  $t$  for each  $n$  can be regarded as an energy level  $\tilde{\epsilon}_n$  of  $n$ th adiabatic state in the presence of a static potential of depth  $\tilde{V} = \tilde{V}_0(1 - e^{-t/\tau})$ . Hence, we can convert the  $E_{\text{tot}}-t$  curve to the  $\tilde{\epsilon}_n - \tilde{V}$  curve, which is identical to Figure 5.
18. L. Allen, J.H. Eberly, *Optical Resonance and Two-Level Atoms*; Dover: NY, **1987**, Chapter 2.

19. S.-I. Chu, *Adv. Chem. Phys.* **1989**, 73, 739.
20. J. Friedel, *Suppl. Nuovo Cimento*, **1958**, 7, 287.
21. F. Rossi, in *Theory of Transport Properties of Semiconductor Nanostructures*; E. Schöll, Ed.; Chapman & Hall: London, **1998**, Chapter 9.
22. W.A. de Heer, W.D. Knight, M.Y. Chou, M.L. Cohen, *Sol. State Phys.* **1987**, 40, 93.
23. S. Bandopadhyay, M. Hentschel, *Phys. Rev. B* **2011**, 83, 035303.
24. G. Bastard, *Wave Mechanics Applied To Semiconductor Heterostructures*; Halsted Press: NY, **1988**.
25. P.W. Langhoff, S.T. Epstein, M. Karplus, *Rev. Mod. Phys.* **1972**, 44, 602.
26. C.L. Hammer, T.A. Weber, *J. Math. Phys.* **1965**, 6, 1591.
27. A. Mandal, K.L.C. Hunt, *J. Chem. Phys.* **2012**, 137, 164109.
28. R. McWeeny, *Phys. Rev.* **1962**, 126, 1028.